IOPscience iopscience.iop.org

Home Search Collections Journals About Contact us My IOPscience

Electron–phonon scattering in molecular electronics: from inelastic electron tunnelling spectroscopy to heating effects

This article has been downloaded from IOPscience. Please scroll down to see the full text article.

2008 New J. Phys. 10 065020

(http://iopscience.iop.org/1367-2630/10/6/065020)

View the table of contents for this issue, or go to the journal homepage for more

Download details:
IP Address: 130.126.32.13
The article was downloaded on 15/05/2013 at 20:03

Please note that terms and conditions apply.

New Journal of Physics
The open-access journal for physics

Electron–phonon scattering in molecular electronics: from inelastic electron tunnelling spectroscopy to heating effects

Alessio Gagliardi[1,2,3], Giuseppe Romano[2], Alessandro Pecchia[2], Aldo Di Carlo[2], Thomas Frauenheim[1] and Thomas A Niehaus[1]

[1] Bremen Center for Computational Materials Science, University of Bremen, D-28359 Bremen, Germany
[2] CNR-INFM Department of Electronics Engineering, University of Rome 'Tor Vergata', Via del Politecnico 1, 00133 Rome, Italy
E-mail: gagliard@bccms.uni-bremen.de and Gagliardi@Ing.uniroma2.it

New Journal of Physics **10** (2008) 065020 (18pp)
Received 31 January 2008
Published 30 June 2008
Online at http://www.njp.org/
doi:10.1088/1367-2630/10/6/065020

Abstract. In this paper, we investigate dissipation in molecular electronic devices. Dissipation is a crucial quantity which determines the stability and heating of the junction. Moreover, several experimental techniques which use inelastically scattered electrons as probes to investigate the geometry in the junction are becoming fundamental in the field. In order to describe such physical effects, a non-equilibrium Green's function (NEGF) method was implemented to include scattering events between electrons and molecular vibrations in current simulations. It is well known that the final heating of the molecule depends also on the ability of the molecule to relax vibrational quanta into the contact reservoirs. A semi-classical rate equation has been implemented and integrated within the NEGF formalism to include this relaxation. The model is based on two quantities: (i) the rate of emission of phonons in the junction by electron–phonon scattering and (ii) a microscopic approach for the computation of the phonon decay rate, accounting for the dynamical coupling between the vibrational modes localized on the molecule and the contact phonons. The method is applied to investigate inelastic electron tunnelling spectroscopy (IETS) signals in CO molecules on Cu(110) substrates as well as dissipation in C_{60} molecules

[3] Author to whom any correspondence should be addressed.

© IOP Publishing Ltd and Deutsche Physikalische Gesellschaft

on Cu(110) and Si(100) surfaces. It is found that the mechanisms of energy relaxation are highly mode-specific and depend crucially on the lead electronic structure and junction geometry.

Contents

1. Introduction

Whether molecular electronics represents the next step in the design of electronic devices is still under debate. However, it is certain that it already now represents one of the most challenging and appealing branches at the frontiers of condensed matter research. This is because it bridges several different areas of investigation: the hybrid system (organic/inorganic interfaces), organic chemistry and surface physics. Moreover, the molecular electronics field features several other topics of broad interest, such as optical excitations [1] and spin–spin correlation effects [2].

The future of molecular electronics depends critically on the possibility of controlling and reproducing device characteristics. One of the most challenging aspects of charge transport in molecular bridges is in this respect the control of power dissipation. By dissipation we mean specifically the energy transfer between flowing charges and the vibrations of the molecular bridge and crystalline leads. Due to the short length of such devices, most of the current flows through the system ballistically, without any energy loss. Only a small fraction undergoes inelastic scattering processes; however, this small fraction of scattered charges can lead to relevant events, which are observed in inelastic electron tunnelling spectroscopy (IETS), or may induce heating processes.

While the former is a positive effect that can be directly used to examine molecular devices, the latter is a negative consequence that often results in degradation of the whole device. For that reason, it is very important to study this scattering process in detail. Several groups have devoted a great deal of effort to the theoretical exploration of dissipation in nanojunctions, using for instance model Hamiltonians [3, 4], or atomistic simulations [5, 6]. For an extended review on the subject, see [7].

A crucial parameter for the computation of molecular heating is the rate of phonon relaxation into the reservoirs. Most models include electron–phonon couplings to account for the interaction between electrons and the vibration of the molecule and employ empirical parameters to describe the damping of the vibrational energy into the heat bath represented by the leads. Our method, based on non-equilibrium Green's functions (NEGF), allows the computation of electron–phonon coupling matrices from first principles, assuming a harmonic

approximation, and evaluation of the molecular phonon lifetime without the use of any phenomenological parameter.

The code includes two mechanisms for dissipation of phonons: a phonon–phonon dissipation effect, in which a vibrational quantum on the device excites a phonon in the crystalline contacts, and an electron–hole excitation process, whereby a vibrational quantum excites an electron in the leads creating an electron–hole pair. Several other processes can play an important role in the final dissipation of heat in the device. For example, anharmonic processes can be relevant. However, at this level of approximation, the two damping mechanisms can be used to establish a classical rate equation. This equation is coupled with the Green's function treatment of the electron–phonon scattering in the device. It describes the final non-equilibrium phonon population in the junction under bias and thereby the heating of the molecule between the contacts.

The paper is organized as follows: in section 1 a theoretical view of the method is given. Section 2 is divided into two subsections, the first describing the formalism for the current computation using the Meir–Wingreen formalism as well as the expansion of the self-energy for the electron–phonon interaction and the second subsection describes the semi-classical rate equation mentioned above. Section 3 is devoted to the application of the formalism to different systems: (i) the simulation of IETS signals of CO molecules on copper substrates and (ii) a comparison of power dissipation of fullerene molecules on metallic and semiconducting substrates.

2. Theoretical method

2.1. Transport formalism

Our calculations are performed using the Green's function density-functional tight-binding (gDFTB) program [8]–[10]. It implements an NEGF technique to calculate the current in molecular devices taking inelastic effects into account. The zero-order Hamiltonian for the system, including the two contacts, is computed *a priori* using the code DFTB, a DFTB method [11, 12] implemented in a local-orbital basis set. The method allows the determination of inter-atomic forces by constructing appropriate repulsive potentials fitted against full density functional theory (DFT) calculations of suitable reference systems. Within DFTB the electron–phonon coupling matrix elements can be obtained by expanding the Hamiltonian and overlap matrix elements to first order in the atomic displacement. We should spend some words to clarify what we mean by 'phonon' in the unusual context of molecular electronics. In this paper, we will use the same term for two different, but related, concepts in order to simplify the notation. If we are talking about vibrations in the active region of the device, a phonon is the localized vibration obtained by diagonalizing the Hessian matrix of the extended molecule only. These vibrations are coupled with an external bath represented by the motion of the ions of the two semi-infinite leads; these vibrations are real phonons in the usual sense of the literature. Sometimes, the localized vibrations are called 'vibrons' in order to stress the difference between the localized and the bath vibrational modes.

The basic equation for the current in non-equilibrium conditions is given by the well-known Meir–Wingreen equation [13]:

$$I = \frac{2e}{h}\int_{-\infty}^{+\infty} \mathrm{Tr}[\Sigma_{\mathrm{L}}^{<}(E)G^{>}(E) - \Sigma_{\mathrm{L}}^{>}(E)G^{<}(E)]\,\mathrm{d}E, \tag{1}$$

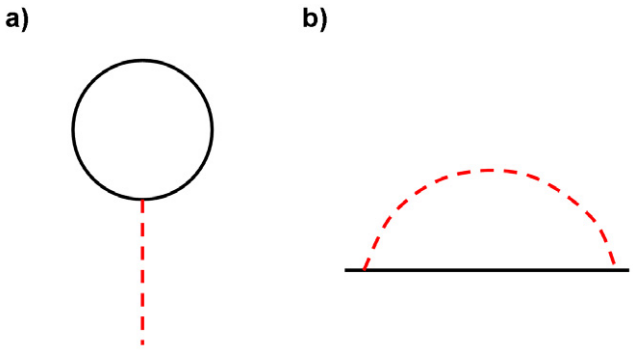

Figure 1. (a) Tadpole diagram for the phonon self-energy. (b) Rainbow diagram. The black continuous lines stand for electron propagators and the red broken lines stand for phonon propagators.

where the two correlation propagators, lesser (greater), $G^{<(>)}(E)$ describe the dynamics of the charges in the device region and the lesser (greater) self-energies $\Sigma_L^{<(>)}(E)$ describe the inflow (outflow) of charges from (into) the contact into (from) the device. Only the left lesser and greater self-energies are required because in steady state the left current is equal in magnitude (and of opposite sign) to the current flowing into the right contact. The correlation functions are defined as:

$$G^{<,>}(E) = G^r(E)[\Sigma_{\mathrm{L}}^{<,>}(E) + \Sigma_{\mathrm{R}}^{<,>}(E) + \Sigma_{\mathrm{ph}}^{<,>}(E)]G^a(E). \tag{2}$$

The first two terms which appear in the brackets of (2) are the lesser (greater) self-energies which take the non-equilibrium distribution of electrons into account, that is induced by the open boundary conditions:

$$\Sigma_{\mathrm{L,R}}^{<,>}(E) = \eta^{<,>}(-2\,\mathrm{Im}\{\Sigma_{\mathrm{L,R}}^r(E)\}) = \eta^{<,>}\Gamma_{\mathrm{L,R}}, \tag{3}$$

where $\eta^{<(>)}$ is equal to $\mathrm{i}f_{\mathrm{L,R}}(-\mathrm{i}(1-f_{\mathrm{L,R}}))$, with the Fermi distribution functions f for the contacts. The third term $\Sigma_{\mathrm{ph}}^{<,>}$ introduces the inelastic scattering in the current and embodies the electron–phonon interaction. It is computed using a Dyson perturbation expansion truncated at first order (the Born approximation) as the interaction between the electrons and phonons is assumed to be weak.

The first order of perturbation expansion contains two contributions. They are represented by two diagrams: the so-called rainbow diagram and the tadpole diagram (see figure 1). We calculate only the rainbow diagram and neglect the tadpole, as will be explained later, which leaves us with the following equation for the phonon self-energy:

$$\Sigma_{\mathrm{ph}}^{<,>}(E) = \sum_q \frac{\mathrm{i}}{2\pi}\int_{-\infty}^{\infty} \alpha_q G_0^{<,>}(E-E')\alpha_q D_{0,q}^{<,>}(E')\,\mathrm{d}E, \tag{4}$$

where α_q is the electron–phonon coupling matrix defined by

$$\alpha_{\mu\nu}^q = \sum_i \sum_{\mu\nu} \sqrt{\frac{1}{2M_i\omega_q}} \left(\frac{\partial H_{\mu\nu}}{\partial Q_{qi}} - \sum_{\sigma\lambda} \frac{\partial S_{\mu\sigma}}{\partial Q_{qi}} S_{\sigma\lambda}^{-1} H_{\lambda\nu} - \sum_{\sigma\lambda} H_{\mu\sigma} S_{\sigma\lambda}^{-1} \frac{\partial S_{\lambda\nu}}{\partial Q_{qi}} \right) e_i^q \tag{5}$$

for a phonon mode of frequency ω_q. Here, $H_{\mu\nu}$ denotes the molecular Hamiltonian and $S_{\mu\nu}$ the orbital overlap. The term Q_{qi} is the normal mode coordinate for the ith ion of mass M_i and e_i^q

is the corresponding eigenvector component [14]. The $D_{0,q}(E')$ are the zero-order correlation functions of the qth phonon mode:

$$\begin{aligned} D^{<}_{0,q}(E) &= -2\pi \mathrm{i}[(N_q+1)\delta(E+\omega_q)+N_q\delta(E-\omega_q)], \\ D^{>}_{0,q}(E) &= -2\pi \mathrm{i}[(N_q+1)\delta(E-\omega_q)+N_q\delta(E+\omega_q)], \end{aligned} \tag{6}$$

where N_q is the number of phonons for the qth vibrational mode. At this level of approximation the phonons are considered to be a collection of Einstein oscillators of frequency ω_q, i.e. their lifetimes are neglected. This is not inconsistent, since the spectral broadening resulting from the lifetimes is quite small and a smaller contribution in the integration in (4), which is greatly simplified taking advantage of the delta functions in (6).

Self-consistency in the electron–phonon interaction is obtained when the renormalized Green's functions ($G^{<,>}$) are used in (4). At the same time, $G^{r,a}$ are renormalized by the phonon self-energies, $\Sigma^{r,a}$. In our treatment, we include only the imaginary parts of the phonon self-energies, obtained from the relationship $\mathrm{Im}\{\Sigma^{r,a}\} = \frac{1}{2}[\Sigma^{>}_{\mathrm{ph}} - \Sigma^{<}_{\mathrm{ph}}]$. Since we are mainly interested in the electron lifetime and consider only weak electron–phonon couplings, the real part of $\Sigma^{r,a}_{\mathrm{ph}}$, responsible for a polaronic shift, is neglected. Consequently, we also neglect the first-order tadpole diagram, which gives a contribution to the real part only. The self-consistent Born approximation (SCBA) is usually reached by implementing an iterative loop. In some cases, good results can also be achieved by neglecting the self-consistent loop and leaving the propagators and self-energies at the lowest order (BA), which is however not the approach used in this study.

2.2. Semi-classical phonon relaxation rate

When a bias is applied and a current starts to flow, the interaction between electrons and phonons moves the population of phonons in the device out of equilibrium. That is, the distribution of phonons is no longer a simple Bose–Einstein distribution due to scattering processes. Moreover, the presence of the leads allows the relaxation of phonons from the device into the contacts. In order to describe this process, a semi-classical rate equation has been implemented [9]:

$$\frac{\mathrm{d}N_q}{\mathrm{d}t} = R_q - J_q[N_q - n_q(T_0)], \tag{7}$$

where R_q is the net rate of phonons created in mode q and J_q is the decay rate of phonons into the bath by phonon–phonon interactions. As will be shown later, the electron–hole excitation is already contained in the R_q. The first term in (7) contains the net emission of molecular phonons due to electron–phonon coupling, while the second tends to restore the population N_q to the equilibrium Bose–Einstein distribution, $n_q(T_0)$, characterized by the contact temperature, T_0.

Once a steady state is reached, the phonon distribution for the qth mode reduces to

$$N_q = n_q(T_0) + R_q/J_q. \tag{8}$$

In other words, at steady state the number of phonons emitted must balance the number of phonons dissipated into the contact reservoirs. It is possible to demonstrate that [9]:

$$R_q = [(N_q+1)E_q - N_q A_q], \tag{9}$$

where E_q and A_q are interpreted as an emission and an absorption rate due to electron–phonon coupling. The two coefficients can be directly extracted from the formula for the dissipated power [15]:

$$P_q = \frac{2}{h}\int_{-\infty}^{+\infty} \mathrm{Tr}[\Sigma_{\mathrm{ph}}^{<}(E)G^{>}(E) - \Sigma_{\mathrm{ph}}^{>}(E)G^{<}(E)]E\,\mathrm{d}E. \tag{10}$$

After some manipulations, we get for A_q and E_q:

$$E_q = \frac{2}{h}\int_{-\infty}^{+\infty} \mathrm{Tr}[\alpha_q G^{<}(E+\omega_q)\alpha_q G^{>}(E)]\,\mathrm{d}E \tag{11}$$

and

$$A_q = \frac{2}{h}\int_{-\infty}^{+\infty} \mathrm{Tr}[\alpha_q G^{<}(E-\omega_q)\alpha_q G^{>}(E)]\,\mathrm{d}E. \tag{12}$$

Both the absorption and emission coefficients can be decomposed into a sum of different contributions. They represent electron–phonon interactions between the electrons in the whole system, device and contacts, with vibrations in the device region only. We show only the absorption coefficient (a similar argument holds for the emission coefficient E_q) within the BA and for $T = 0$. Expanding the absorption term in (12) with (3), we obtain

$$\begin{aligned}
A_q &= \frac{2}{h}\int_{-\infty}^{+\infty} \mathrm{Tr}[\alpha_q G^{<}(E-\omega_q)\alpha_q G^{>}(E)]\,\mathrm{d}E \\
&= \frac{2}{h}\int_{\mu_{\mathrm{L}}}^{\mu_{\mathrm{L}}+\omega_q} \mathrm{Tr}[\alpha_q A_{\mathrm{L}}(E-\omega_q)\alpha_q A_{\mathrm{L}}(E)]\,\mathrm{d}E \\
&\quad + \frac{2}{h}\int_{\mu_{\mathrm{R}}}^{\mu_{\mathrm{L}}+\omega_q} \mathrm{Tr}[\alpha_q A_{\mathrm{L}}(E-\omega_q)\alpha_q A_{\mathrm{R}}(E)]\,\mathrm{d}E \\
&\quad + \Theta(\mu_{\mathrm{R}}+\omega_q-\mu_{\mathrm{L}})\frac{2}{h}\int_{\mu_{\mathrm{L}}}^{\mu_{\mathrm{R}}+\omega_q} \mathrm{Tr}[\alpha_q A_{\mathrm{R}}(E-\omega_q)\alpha_q A_{\mathrm{L}}(E)]\,\mathrm{d}E \\
&\quad + \frac{2}{h}\int_{\mu_{\mathrm{R}}}^{\mu_{\mathrm{R}}+\omega_q} \mathrm{Tr}[\alpha_q A_{\mathrm{R}}(E-\omega_q)\alpha_q A_{\mathrm{R}}(E)]\,\mathrm{d}E,
\end{aligned} \tag{13}$$

where μ_{L} and μ_{R} are the chemical potentials of the left and right contacts, respectively, and the right contact is at higher potential V, i.e. $\mu_{\mathrm{L}} > \mu_{\mathrm{R}}$. Equation (13) looks like a sum of terms of the kind $\mathrm{Tr}[\alpha_q A_\beta \alpha_q A_\lambda]$, where the β and λ indices run over the left and right contacts and the $A_{\mathrm{L,R}}$ are equal to

$$A_{\mathrm{L,R}} = G^r \Gamma_{\mathrm{L,R}} G^a. \tag{14}$$

The different contributions in (13) can be easily interpreted following figure 2. The first two terms, which include different indices L and R, represent scattering processes where an electron flowing from one contact to the other absorbs a phonon in the device region (figure 2(a)). These two terms contribute to the inelastic current. On the other hand, the terms that couple one contact with itself describe a process in which an electron in the contact is emitted and sent back to the same contact (figure 2(b)). These latter scattering processes cannot contribute to the current due to the fact that no net charge travels across the device. However, this mechanism contributes to

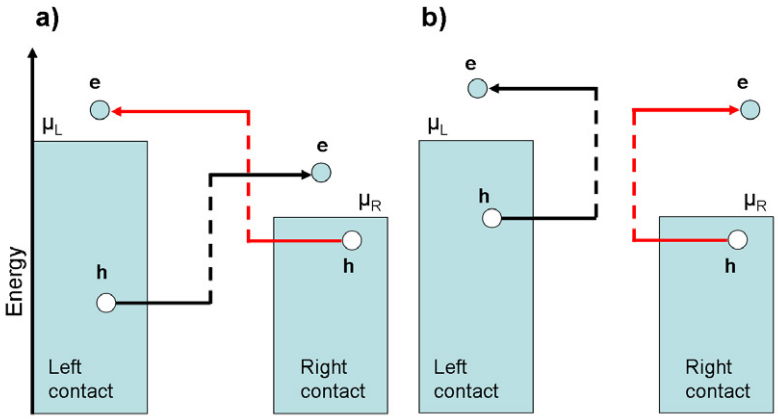

Figure 2. (a) Inelastic processes that contribute to the current: an electron emitted from one contact undergoes a scattering process in the device region and relaxes thereafter into the other contact. (b) Inelastic processes that do not contribute to the current: an electron emitted from one contact undergoes a scattering process in the device region and relaxes thereafter into the same contact.

the final phonon rate entering the absorption coefficient. These terms describe the electron–hole damping mechanism[4].

The final number of phonons for a mode q at steady state can be obtained by substituting (9) in (8), obtaining:

$$N_q = \frac{n_q(T_0)J_q + E_q}{J_q + A_q - E_q}. \tag{15}$$

Since the terms A_q and E_q depend on the population N_q via the Green's function $G^{<,>}$, which contains the phonon propagator, a self-consistent loop is necessary.

Once the phonon populations are computed, we define an effective temperature, obtained by redistributing the energy stored in the molecular vibrations into a Bose–Einstein distribution $n_q(T_\mathrm{m})$ with temperature T_m. This procedure is equivalent to imposing energy conservation,

$$\sum_q \omega_q n_q(T_\mathrm{m}) = \sum_q \omega_q N_q. \tag{16}$$

This definition of a local temperature turns out to be helpful in the analysis of molecular stability.

The last crucial parameter of the formalism is J_q, which represents the phonon–phonon relaxation into the contacts [17]. The evaluation of this parameter from first principles is quite complicated, since several different processes can play a fundamental role in the final definition of the J_q coefficients. The gDFBT code allows for two ways of introducing it, firstly as a phenomenological parameter derived from experiments; secondly, it can be determined directly, starting from the Hessian matrix of the entire system (contact–molecule–contact), which is also the approach pursued here. The calculation is performed by setting up the full Hessian and partitioning it in the same way as the Hamiltonian, namely into device region and contacts.

[4] It should be noted that electronic excitation in the leads due to absorption of infrared emission potentially emitted by the vibrating molecule is not captured by our approach [16].

A Green's function is then built for the vibrational eigensystem:

$$\sum_j \mathcal{H}_{ij} e_j^q = \sum_j \mathcal{M}_{ij} e_j^q \omega_q^2, \tag{17}$$

using open boundary condition as usual. In the previous equation, $\mathcal{H}_{ij}$ is a matrix element of the Hessian, e_j^q are the normal modes of vibration, $\mathcal{M}_{ij}$ is the mass matrix element and ω_q is the frequency of the mode. From (17) it is possible to construct a self-energy for the phonons, the imaginary part of which, as for the electron part, can be used to extract the phonon relaxation lifetime into contact phonons [9].

This is essentially a Fermi golden rule treatment including first-order one phonon to one phonon decay processes. It neglects a large number of other decay channels, for example related to anharmonic effects. In particular, high-frequency modes do not couple directly with the phonon band of the contacts, meaning that only one phonon to many phonons decay processes are relevant in describing such relaxation mechanisms. Some of these effects can be partially included by defining an effective phonon density of the contact modes. The formal Green's function for the phonons is

$$G_p^r(\omega^2) = \frac{1}{\mathcal{M}_i \omega^2 - \mathcal{H}_M - \Pi_{\mathrm{L}}^r(\omega^2) - \Pi_{\mathrm{R}}^r(\omega^2)}, \tag{18}$$

where the self-energies $\Pi_{\mathrm{L,R}}^r(\omega^2)$ map the infinite contacts into the finite portion of the device. The real part of the self-energies represents a shift of the frequencies of the normal modes of the extended molecule induced by the coupling of that region with the bath, the imaginary part instead describes the phonon–phonon decay process J_q. In order to simplify the calculation in the rest of the paper, we have computed only the imaginary part and neglected the real part, which gives anyway a small correction to the frequencies. The local phonon density of states (LDOS) projected on the molecule can then be computed from the retarded Green's function,

$$\rho(\omega^2) = -\frac{1}{\pi} \mathrm{Tr}[\mathrm{Im}\{G_p^r(\omega^2)\}\mathcal{M}]. \tag{19}$$

3. Results and discussion

3.1. IETS of CO molecules on the Cu(110) surface

In this section, we apply the electron–phonon code to investigate IETS measurements of a CO molecule on the Cu(110) surface. The advantage of IETS is that inelastically scattered electrons can be used directly as probes to uncover many properties of the device [18]–[20]. While this approach is quite old [21], it has not been popular until now. This is primarily because, compared with other more traditional spectroscopic techniques like infrared, HREELS or Raman spectroscopy, IETS requires a more complicated setup. In fact, the sample must be contacted by two electrodes. Moreover, it is difficult to isolate the influence of the environment and local structural variations on the final spectrum. While the advent of experimental molecular electronics has solved the first issue, the influence of the environment is still under debate [20, 22]. Many groups have investigated the rigorous formalism that underlies IETS measurements [14], [23]–[27] and have investigated environmental effects [10, 20], [28]–[31].

As pointed out before, the broadening of spectral lines of the molecule depends mainly on two processes related to phonon decay: the excitation of a phonon in the leads (PP process) or the excitation of an electron–hole pair that relaxes in the contact afterwards (EH process).

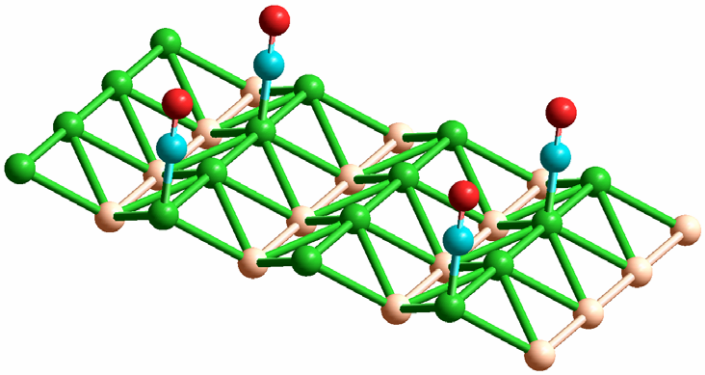

Figure 3. Geometry of the CO molecules on top of the Cu(110) surface. Carbon is in blue and oxygen is in red. The upper atoms of copper are in green (dark), while the atoms in the trench are in pink (light).

The relaxation rate of a single phonon in an electron–hole in the contact for a mode q can be computed using the first term of equation (13), assuming that the left contact represents the substrate:

$$R^q_{\mathrm{EH}} = \frac{2}{h}\int_{\mu_{\mathrm{L}}}^{\mu_{\mathrm{L}}+\omega_q} \mathrm{Tr}[\alpha_q A_{\mathrm{L}}(E-\omega_q)\alpha_q A_{\mathrm{L}}(E)]\,\mathrm{d}E. \tag{20}$$

The first mechanism (PP) is particularly relevant when the mass of the atoms comprising the molecule is of the same order as the mass of the lead atoms. In that case, a vibration of the molecule can effectively excite a vibration in the leads. For that reason one expects that this mechanism is especially efficient for contacts made of light elements, like silicon for example. On the other hand, for heavier elements, like metallic leads, the PP process is strongly suppressed, since the cut-off frequency of the phonon band of the leads (the Debye frequency) is much lower than the entire spectrum of the molecule. The second mechanism, EH, becomes the dominating process. This second mechanism is instead absent in semiconductors due to the large energy gap, which forbids the excitation of electrons from the valence band into the conduction band.

The CO system has been investigated in a large spectrum of different conditions, for instance on different samples. Here, the scanning tunelling microscope (STM) configuration permits the addition of another contact and allows for transport experiments in order to obtain the IETS signal. IETS measurements for different surfaces have been performed by many groups. In particular, Lauhon and Ho [32] have studied CO on 110 and 100 surfaces. We concentrate on the first surface only (see figure 3). In our investigation, we first relaxed a self-assembled monolayer of CO molecules on top of a Cu(110) copper surface, using the DFTB method mentioned above. On the Cu(110) surface, CO molecules relax vertically on top of the upper copper atoms in a (2×1) supercell [33]. The computed CO bond length is 1.156 Å and the copper molecule distance is found to be 1.729 Å. In order to compute the IETS signal, a second electrode, besides the copper substrate, has been added. It was represented by a pyramid of 14 copper atoms.

A CO molecule on Cu(110) has six vibrational modes: the C–O stretch (ν_1), the doubly degenerate hindered rotation (ν_2), the CO–Cu stretch (ν_3) and, finally, the doubly degenerate hindered translation (ν_4). The presence of the substrate slightly breaks the degeneracies, but the

Table 1. Modes of vibration of CO on the Cu(110) substrate. The frequencies in wavelength are compared with experimental results.

Mode	DFTB (cm^{-1})	Exp. (cm^{-1})
ν_1	1854	2073[a]
ν_2	370	293[a]
ν_3	301	–
ν_4	37	–

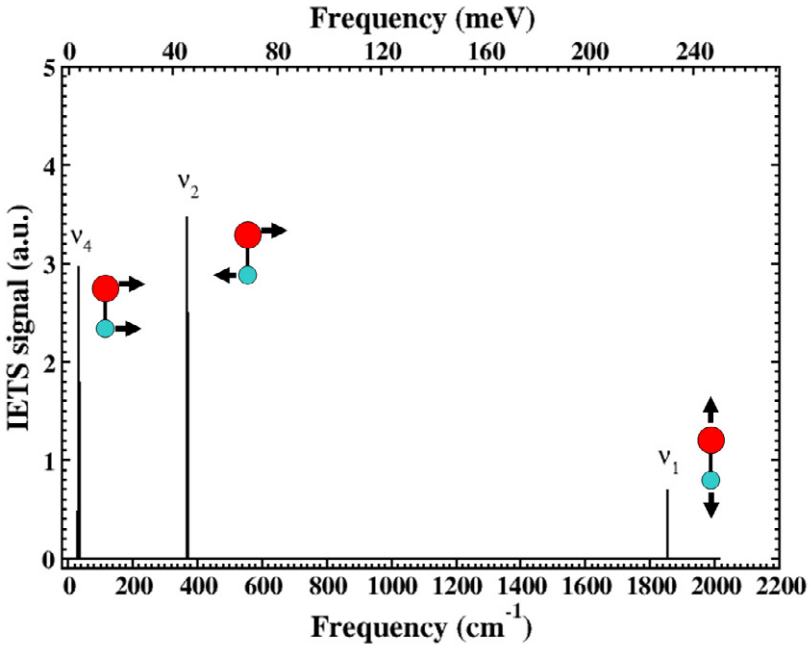

Figure 4. Computed IETS intensities for the CO/Cu(110) system. Close to every mode a sketch of the corresponding atomic motion is given. The upper atom (red) is the oxygen and the lower (blue) is the carbon.

effect is pretty small and can be discarded. In table 1, the frequencies of the different modes are reported in comparison with experiments.

The IETS signal computed according to the formalism presented in section 2.1 is shown in figure 4, together with a sketch of the different modes of vibration. There are only three IETS active modes in CO on Cu(110) as also pointed out by Lauhon and Ho [32].

An important point is how the different vibrational modes relax into the sample. Also, even if the EH mechanism is more efficient than the PP one for metallic substrates, the PP relaxation can play an important role for low-frequency modes. In table 2, the lifetimes of different modes are shown. In the second column, the lifetimes obtained by DFTB are compared with the experimental values given in the last column.

From table 2, we can see that, apart from mode ν_3, all the modes show lifetimes of the order of a few picoseconds, if not less (ν_1). The behaviour of the lifetimes can be traced back to the EH and PP mechanisms as shown in figure 5.

Table 2. Lifetimes in picoseconds for the four modes of vibration. DFTB calculation compared with experimental results. The experimental results were obtained for CO on different substrates, like Cu(100), but similar values are expected also for the surface at hand, see [39].

Mode	DFTB (ps)	Exp. (ps)
ν_1	0.4	2[a]
ν_2	6.14	1[b]
ν_3	124.2	>10[c]
ν_4	4.9	–

[a] Morin *et al* and Harris *et al* [34, 35].
[b] Hirschmugl *et al* [36, 37].
[c] Ryberg *et al* [38].

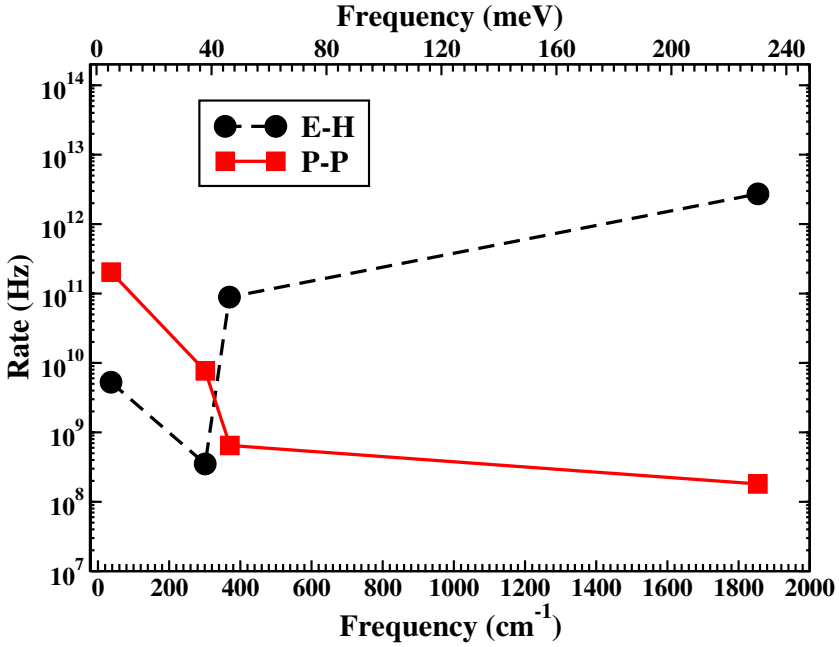

Figure 5. Rate values for the four modes of vibrations. The black (broken) line stands for the EH rate and the red (continuous) line for the PP rate.

In figure 5, the rates of phonon relaxation are plotted in logarithmic scale for the PP and EH contributions separately. The final lifetime, τ, is defined as:

$$\tau = \frac{1}{R_{\mathrm{EH}} + R_{\mathrm{PP}}}, \tag{21}$$

where R_{EH} and R_{PP} are the rates for the two relaxation mechanisms, EH and PP. We see that there is a fundamental step in the relaxation rates for the modes below 400 cm^{-1} and beyond this threshold. The PP rate is particularly high in that region. The explanation is that the edge of the dispersion function for phonons of copper is exactly around 400 cm^{-1} (see figure 7(b)). This results in a stronger coupling between modes below that threshold with the modes of the metallic surface.

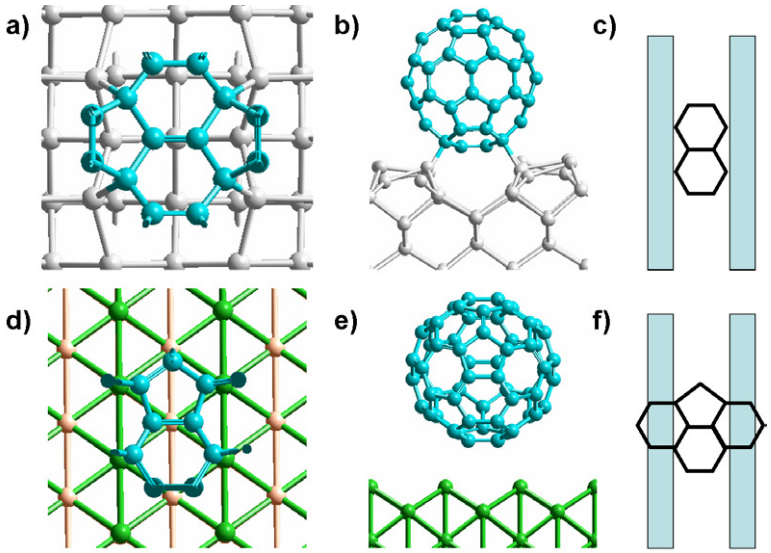

Figure 6. Geometries of C_{60} relaxed on two different surfaces. (i) Si(100): (a) top view of the lowest fullerene atoms close to the silicon surface, (b) side view and (c) sketch of the bonding site. (ii) Cu(110): (d)–(f) the same as for silicon.

More complicated is the explanation for the trend of the EH rate. The behaviour of this rate is related to (13), in particular to the second term in that equation. The final EH rate depends on several contributions, i.e. the frequency ω_q, the partial density of states A_L and A_R, see (14), and the electron–phonon couplings α_q. All these quantities contribute to the final value of the relaxation rate. However, in the specific case under investigation, we can assume that the two quantities, A_L and A_R, are almost constant. This is a consequence of the alignment of the CO states with the s-band of copper. The s-band is almost constant in energy for a large energy interval and so there is also not a dramatic change of $A_{L,R}$ around the Fermi energy ($E_f \pm \omega_q$). Consequently, the EH relaxation rate depends on ω_q and α_q only. The frequency ω_q determines the interval of integration in (13). This means that there are more ways for phonons of high energy to excite electrons in the metal and that these modes are more easily damped in electron–hole pairs compared with low-frequency modes.

This explanation describes well the trend of all the modes, apart from ν_3 which remains an anomaly. For that mode, the electron–phonon coupling becomes relevant. From the IETS signal, figure 4, it is clear that mode ν_3 interacts very poorly with electrons, which directly leads to a small electron–hole relaxation rate.

It is clear that further investigations will be important to understand the limitations and the strengths of the formalism in order to make more accurate predictions. Other groups have tried to estimate phonon relaxation rates for CO and similar molecule vibrations on other substrates [39]–[42].

3.2. Dissipation of C_{60} molecules on metallic Cu(110) and silicon Si(100) surfaces

In this section, we explore the heating of a molecular junction induced by electron–phonon scattering [43]. The systems under investigation are a fullerene molecule on Cu(110) and Si(100) surfaces. The geometries of the two structures, fully relaxed at the DFTB level, are shown in figure 6. The final result for the C_{60} on Cu(110) is in very good agreement

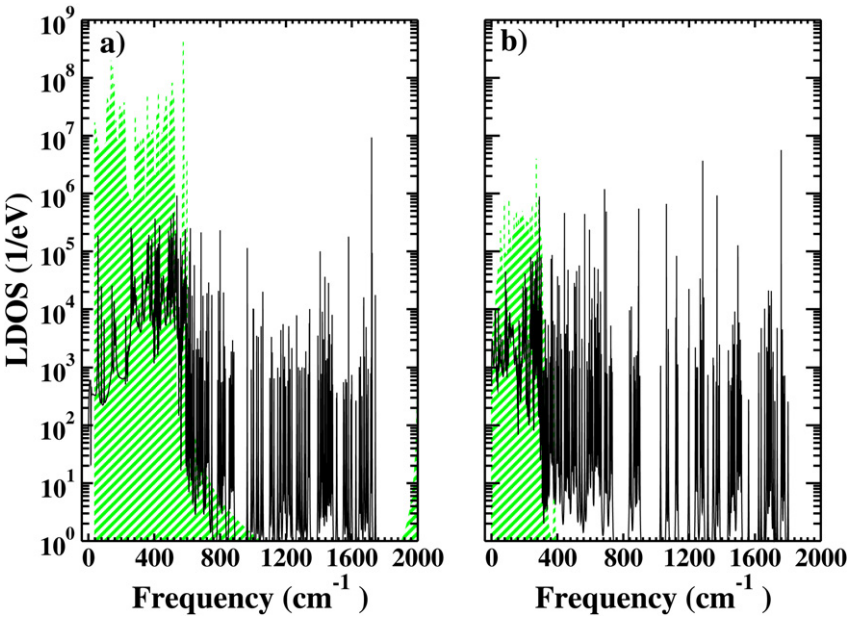

Figure 7. The phonon LDOS for the two systems, (a) C_{60} on Si(100) and (b) C_{60} on Cu(110). The black line represents the LDOS with broadening induced by coupling with the surface modes. In the background, the shaded areas represent the phonon density of states for the isolated substrates.

with experimental results [44, 45]. The distance between the fullerene and copper atoms is about 2.85 Å, while the distance between the fullerene and the copper plane is 2.3 Å, indicating physisorption. Adding an empirical van der Waals correction to the DFTB energy expression [46] led to negligible changes in the relaxed geometry. The surface reconstruction on copper is mostly absent, as predicted in [47]. Reconstruction is more relevant for C_{60} on silicon surfaces. As depicted in figures 6(a)–(c), dimers of the silicon surface are distorted by the presence of the fullerene. The length of the covalent bond between the molecule and the surface is 1.99 Å and the distance between the molecule and the surface is found to be 0.96 Å. The geometry of minimum energy in DFTB is supported by the theoretical results obtained by Martsinovich *et al* [48] and Hobbs *et al* [49].

The coupling between the phonons of the substrate and the vibrations of the molecule can be quantified by the LDOS, as obtained from (19) and shown in figure 7.

In the background, also the surface density of states for the phonons of the isolated substrates is given. The silicon substrate (figure 7(a)) has a Debye frequency of 650 cm^{-1}, while for the much heavier copper atoms it is only 400 cm^{-1} (figure 7(b)). The broadenings of the molecular vibrations are directly proportional to the decay rates into the contact reservoirs, the J_q coefficient of (7). It is easy to observe that the broadening becomes very narrow beyond the Debye frequency. Moreover, as expected, the broadening induced by the silicon substrate for the modes below the Debye frequency is substantially larger (corresponding to a rate of 10^{12} Hz) than the broadening for the copper substrate (10^{11} Hz). This is a straightforward consequence of the higher mass of copper compared with silicon.

In order to compute the current through the system a second contact has been added to the geometry. A metallic STM tip was used, represented by a copper atom coupled with a free

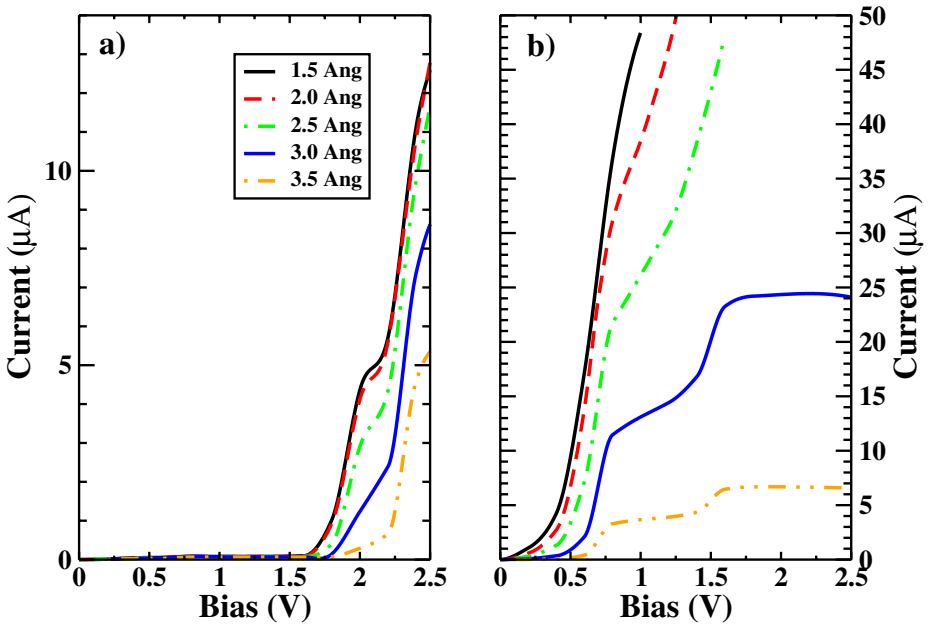

Figure 8. Calculated I–V characteristics for varying tip–sample distance. (a) C_{60} on Si(100). (b) C_{60} on Cu(110).

electron gas reservoir. In all the simulations the substrate and tip were assumed to be at $T = 0$ K. The I–V characteristics are plotted in figure 8 for different tip–molecule distances.

The dramatic difference between the two systems is evident in the current. In silicon, the energy gap determines the final shape of the I–V curve, which rises for a bias beyond 1.75 V when the conduction band of the sample enters in conduction. Conversely, for the C_{60} on copper, the current increases very quickly and shows steps at 0.8 and 1.2 V, where the LUMO (lowest unoccupied molecular orbital) and the LUMO + 1 of the C_{60} conduct resonantly. These steps are more evident for larger distances when the electronic broadening is less pronounced.

The temperature, computed using (16), can be evaluated for both the systems and compared with the internal energy U_{m} stored in the molecule. We find that the power dissipated into the molecule P_{m}, which is related to the internal energy U_{m}, is smaller than the total power, i.e. $P = IV$, by roughly a factor of a thousand. This shows that the electron–phonon interaction is weak and provides a justification for the perturbative approach to the problem via SCBA.

For both the systems under investigation, the tip–molecule distance (Z) and the bias (V) control the temperature; however, in the case of the silicon substrate, the energy gap also plays an important role. The temperature of C_{60} on silicon is shown in figure 9 together with the electronic LDOS of the molecule. Due to the energy gap the molecular states of C_{60} couple only weakly with the substrate, giving rise to a sharp, delta-like shape of the states in the LDOS. This small broadening is reflected in the low conductivity in the gap region[5]. This allows a small tunnelling current also in the gap region of about 0.1 μA. Steps in the temperature are observed after resonances of the electronic LDOS enter the conduction window. However, due to energy conservation, the electron–phonon emission from (11) is related to the Green's function

[5] The silicon substrate has in fact been made conducting also at small bias by doping it, p-type, with a concentration of 10^{19} holes cm^{-3}.

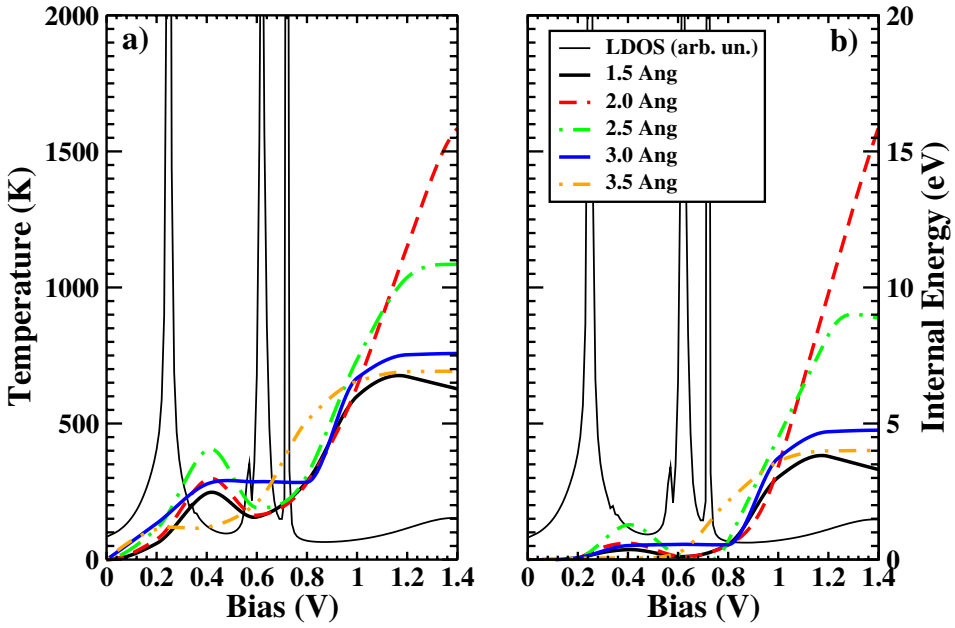

Figure 9. C_{60} on Si(100): (a) temperature in the junction for different tip–molecule distances; (b) internal energy, U_m, for different tip–molecule distances.

evaluated at an energy shifted by ω_q. Hence, the resonance is fully effective only at a bias beyond $V_{res} + \omega_{max}$, where V_{res} is the bias at which the resonance enters in conduction and ω_{max} is the largest frequency of the molecule. In our fullerene case, this leads to a shift of 0.2 V between V_{res} and the energetic position of the temperature step.

Similar behaviour can be noticed for the fullerene on the copper substrate. In particular, there is a large increase in temperature and internal energy (figure 10(a)) around 1 V, that is, 0.2 V after the first resonance at 0.8 V enters in conduction.

Comparing the two temperature curves, figures 9 and 10, some important differences can be noticed. The temperature for the copper substrate increases very fast. This is mainly a consequence of the larger density of states, which results in larger conductivity. A larger current means higher inelastic scattering and eventually power dissipation. Moreover, the weak bonding between C_{60} and copper as well as the small phonon coupling J_q increases the heating.

One could expect that the C_{60} on silicon heats up more slowly, because the total current is lower than on a metal. However, if we careful watch the two curves, we find that this conclusion is deceptive. For example, at 1 V the temperature is 700 K against 1950 K on copper for a tip–molecule distance of 2 Å. However, the current is 40 μA on copper compared with 0.1 μA on silicon, so 400 times larger. The reason for this discrepancy can be traced back to the second damping mechanism, i.e. electron–hole pair excitations. In metal this effect is quite relevant and cools the molecule down. On the other hand, on silicon the EH mechanism in the substrate is not active and the heating, despite a stronger bonding and a larger phonon coupling, is faster.

Further important evidence for the relevance of the electron–hole mechanism can be seen in the temperature curve for silicon, figure 9. Even though it is impossible to damp phonons into the silicon by forming EH pairs due to the energy gap, this can occur in the metallic tip. Hence, one should expect a dramatic effect on the temperature when the tip–molecule distance

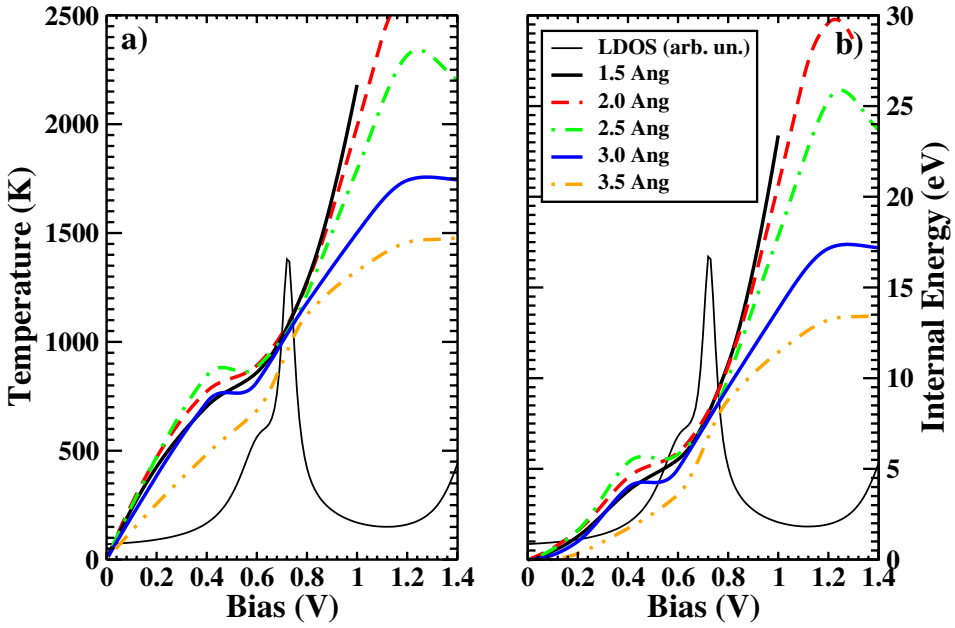

Figure 10. C_{60} on Cu(110): (a) temperature in the junction for different tip–molecule distances; (b) internal energy, U_m, for different tip–molecule distances.

is modulated. Increasing the distance has two opposite effects on the temperature: firstly, it is reduced since the tunnelling current is lowered and, secondly, heating is increased because the EH damping mechanism is distance suppressed. In the case of a metal (figure 10), the first process dominates and the heating goes immediately down. On silicon instead, the temperature first goes up, between 1.5 and 2.0 Å, showing that the reduction due to the EH creation is more relevant and, thereafter, beyond 2.0 Å, the temperature goes down again, like on metals, showing that the lowering of the current is now dominating the heating.

A final remark is devoted to the definition of the molecular temperature T_m, (16). The non-equilibrium condition means that there is no thermodynamic equilibrium and so no well-defined temperature for the system. However, as shown in figures 9 and 10, the temperature T_m follows perfectly the internal energy U_m defined as the sum of the energy stored in the vibrations. Similar results have been observed in other systems [17].

4. Conclusion

In this paper, we presented the results of an NEGF formalism used to compute transport properties of molecular junctions including the effects of electron–phonon interactions via an SCBA self-energy. The model also includes a semi-classical rate equation to describe the relaxation mechanisms of the molecular vibrations into the reservoirs. This formalism has been applied to study two cases which are exemplary for the relevant problems that can be faced in molecular electronics with respect to electron–phonon scattering.

The first application was devoted to a study of IETS signals and vibrational lifetimes of CO molecules on Cu(110) substrates. The theory was able to correctly describe the absence of the CO–Cu stretch mode in the spectrum, which is in full agreement with experiments [32].

Regarding the lifetimes, the method shows two different trends for the relaxation related to the dominance of the PP or the EH mechanism. Below the Debye frequency of copper, the PP seems to be more or at least as important as the EH, but beyond that threshold the EH mechanism is dominating.

In the second application, the formalism was used to investigate dissipation effects in fullerene within an STM framework. Two different conditions were studied: when the substrate is semiconducting, Si(100), and when it is metallic, Cu(110). Two parameters were varied to change the current: the applied bias and the tip–molecule distance. In the case of silicon substrates, the energy gap is the preponderant feature in the I–V characteristics.

The steady-state rate of emission and absorption of phonons was used to evaluate the temperature in the junction for both systems. The temperature depends on the equilibrium balance between excitation of phonons in the molecule and relaxation into the contacts. It was shown that the PP process is more efficient on silicon than on copper due to the small mass of silicon compared with copper. However, on silicon the EH mechanism is strongly suppressed. This leads to faster heating of fullerenes on silicon. What preserves the low temperature in silicon is the presence of the energy gap, which strongly reduces the total tunnelling current.

In summary, we find a subtle and complex interplay of the electronic structure (LDOS, lead–molecule coupling and gap) with the phononic structure (e–p coupling and PP mechanism) that may lead to opposite trends in conduction. Atomistic simulations may therefore serve as an important tool to analyse, interpret and understand physically rich data from transport measurements.

References

[1] Galperin M and Nitzan A 2005 *Phys. Rev. Lett.* **95** 206802
[2] Park J *et al* 2002 *Nature* **417** 722
[3] Koch J and Von Oppen F 2005 *Phys. Rev. Lett.* **94** 206804
[4] Galperin M, Nitzan A and Ratner M A 2006 *Phys. Rev.* B **73** 045314
[5] Frederiksen T, Paulsson M, Brandbyge M and Antti-Pekka J 2007 *Phys. Rev.* B **75** 235441
[6] Pecchia A, Di Carlo A, Gagliardi A, Sanna S, Frauenheim Th and Gutierrez R 2004 *Nano Lett.* **4** 2109
[7] Galperin M, Ratner M A and Nitzan A 2007 *J. Phys.: Condens. Matter* **19** 103201
[8] Pecchia A and Di Carlo A 2004 *Rep. Prog. Phys.* **67** 1497
[9] Pecchia A, Romano G and Di Carlo A 2007 *Phys. Rev.* B **75** 035401
[10] Gagliardi A, Solomon G C, Pecchia A, Frauenheim Th, Di Carlo A, Hush N S and Reimers J R 2007 *Phys. Rev.* B **75** 174306
[11] Frauenheim T, Seifert G, Elstner M, Niehaus T, Koeler C, Amkreutz M, Sternberg M, Hajnal Z, Di Carlo A and Suhai S 2002 *J. Phys.: Condens. Matter* **14** 3015
[12] Elstner M, Porezag D, Jugnickel G, Elsner J, Haugk M, Frauenheim T, Suhai S and Seifert G 1998 *Phys. Rev.* B **58** 7260
[13] Meir Y and Wingreen N 1992 *Phys. Rev. Lett.* **68** 2512
[14] Solomon G C, Gagliardi A, Pecchia A, Frauenheim Th, Di Carlo A, Reimers J R and Hush N S 2006 *J. Chem. Phys.* **124** 094704
[15] Datta S 1995 *Electronic Transport in Mesoscopic Systems* (Cambridge: Cambridge University Press)
[16] Persson B N J and Lang N D 1982 *Phys. Rev.* B **26** 5409
[17] Romano G, Pecchia A and Di Carlo A 2007 *J. Phys.: Condens. Matter* **19** 215207
[18] Wang W L, Kretzschmar I and Reed M 2004 *Nano Lett.* **4** 643
[19] Kushmerick J G, Lazorcik J, Patterson C H and Shashidhar R 2004 *Nano Lett.* **4** 639

[20] Wang W, Scott A, Gergel-Hackett N, Hacker C A, Janes D B and Richter C A 2008 *Nano Lett.* **8** 478–84
[21] Jaklevic R C and Lambe J 1966 *Phys. Rev. Lett.* **17** 1139
[22] Yu L H, Zangmeister C D and Kushmerick J G 2007 *Phys. Rev. Lett.* **98** 206803
[23] Lorente N, Persson M, Lauhon L J and Ho W 2001 *Phys. Rev. Lett.* **86** 2593
[24] Mingo N and Makoshi K 2000 *Phys. Rev. Lett.* **84** 3694
[25] Tikhodeev S G and Ueba H 2004 *Phys. Rev.* B **70** 125414
[26] Galperin M and Nitzan A 2004 *J. Chem. Phys.* **121** 11965
[27] Paulsson M, Frederiksen T and Brandbyge M 2006 *Nano Lett.* **6** 258
[28] Troisi A and Ratner M A 2006 *Nano Lett.* **6** 1784
[29] Troisi A and Ratner M A 2006 *J. Chem. Phys.* **125** 214709
[30] Lorente N and Persson M 2000 *Phys. Rev. Lett.* **85** 2997
[31] Yu L H, Zangmeister C D and Kushmerick J G 2006 *Nano Lett.* **6** 2515
[32] Lahuon L J and Ho W 1999 *Phys. Rev.* B **60** 8525
[33] Mehmood F, Kara A, Rahman T S and Bohnen K P 2006 *Phys. Rev.* B **74** 155439
[34] Morin M, Levinos N J and Harris A L 1992 *J. Phys. Chem.* **96** 3950
[35] Harris A L, Levinos N J, Rothberg L, Dubois L H, Dahr L, Shane S F and Morin M 1990 *J. Electron Spectrosc. Relat. Phenom.* **54** 65
[36] Hirschmugl C J, Williams G P, Hoffmann F M and Chabal Y J 1990 *J. Electron Spectrosc. Relat. Phenom.* **54** 109
[37] Hirschmugl C J, Williams G P, Hoffmann F M and Chabal Y J 1990 *Phys. Rev. Lett.* **65** 480
[38] Ryberg R 1990 *J. Electron Spectrosc. Relat. Phenom.* **54** 65
[39] Krishna V and Tully J C 2006 *J. Chem. Phys.* **125** 054706
[40] Head-Gordon M and Tully J C 1992 *Phys. Rev.* B **46** 1853
[41] Head-Gordon M and Tully J C 1992 *J. Chem. Phys.* **96** 3939
[42] Abe A and Yamashita K 1998 *J. Chem. Phys.* **119** 9710
[43] Shulze G *et al* 2008 *Phys. Rev. Lett.* **100** 136801
[44] Fasel R, Aebi P, Agostino R G, Naumovic D, Osterwalder J, Santaniello A and Schlapbach L 1996 *Phys. Rev. Lett.* **76** 4733
[45] Fasel R, Agostino R G, Aebi P and Schlapbach L 1999 *Phys. Rev.* B **60** 4517
[46] Elstner M, Hobza P, Frauenheim T, Suhai S and Kaxiras E 2001 *J. Chem. Phys.* **114** 5149
[47] Murray P W, Pedersen M, Laegsgaard E, Stensgaard I and Besenbacher F 1997 *Phys. Rev.* B **55** 9360
[48] Martsinovich N, Hobbs C, Kantorovich L, Fawcett R H J, Humpry M J, Keeling D L and Beton P H 2006 *Phys. Rev.* B **74** 085304
[49] Hobbs C, Kantorovich L and Gale J D 2005 *Surf. Sci.* **591** 45